Phase diagram of water between hydrophobic surfaces

Kenichiro Koga[a)] and Hideki Tanaka
Department of Chemistry, Okayama University, Okayama 700-8530, Japan

Molecular dynamics simulations demonstrate that there are at least two classes of quasi-two-dimensional solid water into which liquid water confined between hydrophobic surfaces freezes spontaneously and whose hydrogen-bond networks are as fully connected as those of bulk ice. One of them is the monolayer ice and the other is the bilayer solid which takes either a crystalline or an amorphous form. Here we present the phase transformations among liquid, bilayer amorphous (or crystalline) ice, and monolayer ice phases at various thermodynamic conditions, then determine curves of melting, freezing, and solid-solid structural change on the isostress planes where temperature and intersurface distance are variable, and finally we propose a phase diagram of the confined water in the temperature-pressure-distance space. © *2005 American Institute of Physics*. [DOI: 10.1063/1.1861879]

I. INTRODUCTION

Confined water has been less extensively studied than bulk water but it is by no means less interesting or less relevant to us. Confined water exists in biological systems (cell membranes, inner cavities of proteins, etc.), geological materials (clays, rocks, etc.), and synthesized or industrial materials (graphitic microfibers with slit pore, inner space of carbon nanotubes, etc.). Some biological systems become unstable or does not function if confined water is removed. Some important properties of nanostructured materials are highly sensitive to the presence of confined water.

Phase behavior of a fluid is much richer in inhomogeneous systems including confined systems than in the bulk system: such nonbulk systems may exhibit confinement-induced freezing and melting, wetting and drying transitions, and prewetting and predrying transitions. Pioneering and more recent theoretical studies of simple fluids are illuminating in understanding those phenomena.[1–3] Water is a complex fluid in the sense that its intermolecular interaction causes hydrogen bonding and so is highly directional. Therefore its phase behavior in confined geometry can be even more complex than that expected from the intermolecular interactions.

Computer simulation has proved to be a powerful theoretical tool for studying such complex behavior of confined water. There are many computational studies on confined water,[4–12] some of the pioneering works date back to 1980s.[4] One of the earlier computer simulations focusing on liquid-solid phase transitions[13] showed that water between hydrophobic surfaces freezes into a bilayer form of crystalline ice when temperature is lowered under a fixed normal pressure. Structure of the bilayer ice is different from any of the 12 bulk ices but each molecule is hydrogen bonded to its four neighbors as it is in the bulk ices. A few years later it was shown that water confined in a rigid hydrophobic slit pore freezes into the bilayer amorphous solid when temperature is

decreased at a fixed lateral pressure.[14] This phase change is unique in that freezing to and melting of the amorphous solid occur as a first-order phase transition accompanying a large amount of latent heat and structural change. This is an unambiguous demonstration of polyamorphism involving liquid water by computer simulation. The freezing and melting are also observed by changing the distance between surfaces at fixed temperature and fixed lateral or bulk pressure, a result of which is a discontinuous force curve with hysteresis.[15] More recently spontaneous formation of a monolayer ice was found by molecular dynamics (MD) simulations of the TIP5P model water.[16]

Quasi-one-dimensional water, too, exhibits phase transitions qualitatively different from those of the bulk water. The first evidence for such transitions was again obtained from MD simulations combined with free-energy calculations: the simulations demonstrated that water inside a carbon nanotube freezes into four different forms of the ice nanotube, a class of quasi-one-dimensional crystalline ices.[17,18] The predicted formation of the ice nanotube was confirmed by experiments of Maniwa *et al.*[19]

The structure, dynamics, and thermodynamic properties of confined water depend on many factors such as confining geometry and physical and chemical properties of surfaces, and the effect of each factor is as yet little understood. Thus it is sensible to choose and study, among many possibilities, model systems with simpler geometries (e.g., slit and cylindrical pores) and simpler surfaces (e.g., structureless surfaces). Even such simpler systems give rise to at least one additional thermodynamic parameter for specifying a thermodynamic state. Full understanding of the phase behavior of confined water with a given geometry requires exploration of a three-dimensional thermodynamic space (e.g., the *TPx* space, where *x* is a geometrical parameter such as diameter of the pore or separation distance of two surfaces). Here we focus on the quasi-two-dimensional system and examine the phase behavior of water in ranges of the thermodynamic conditions much wider than we have done before.

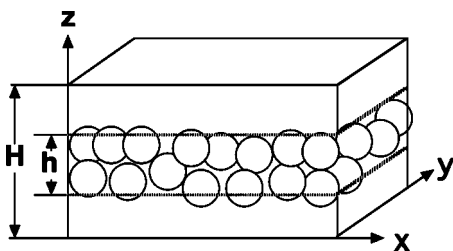[a)]Electronic mail: koga@cc.okayama-u.ac.jp

FIG. 1. Schematic diagram of the system.

II. SYSTEM AND CONDITIONS

As shown in Fig. 1, the model system comprises N molecules in a regular rectangular prism with the dimensions $L_x \times L_y \times H$ in the x, y, and z directions. Periodic boundary conditions are imposed on the x and y directions and two parallel planner walls placed at the top and bottom faces of the prism confine all the molecules between them. The potential energy U of the system is defined as a sum of the potential energy among water molecules and that of the water-wall interaction, both being pair-wise additive:

$$U = \sum_{i=1}^{N-1} \sum_{j=i+1}^{N} \phi(r_{ij}) + \sum_{k=1}^{2} \sum_{i=1}^{N} v(z_{ik}), \qquad (1)$$

where ϕ is the TIP4P water potential[20] multiplied by the switching function that smoothly truncates the potential at $r_c = 8.75$ Å;[21] its argument r_{ij} represents the relative configuration of molecules i and j including their orientations. The pair potential v between molecule i and wall k is a function only of the distance z_{ik} from the wall (the top or base face of the prism) to the position of the oxygen atom of the molecule:

$$v(z_{ik}) = C_9/z_{ik}^9 - C_3/z_{ik}^3. \qquad (2)$$

This Lennard-Jones (LJ) 9-3 potential[22] results from the LJ 12-6 potential integrated over infinite volume of each wall with a uniform density. The parameters C_9 and C_3 are those chosen for the interaction between a water molecule and a "hydrophobic" solid surface.[5] The potential function $v(z)$ is zero at the distance $z_0 = (C_9/C_3)^{1/6} = 2.47$ Å and rapidly increases at shorter distances. In Fig. 1 the dotted lines indicate the surfaces of zero energy $[v(z)=0]$ with a distance h apart whereas the top and base faces of the prism indicate the surfaces of infinite energy with a distance H apart. Note $H - h = 2z_0$. We take h to be the effective width for water and $V = Ah$ to be the effective volume of water, where $A = L_x L_y$ is the area of the bases. Note that one must define, in one way or the other, the effective width or volume as they are not uniquely defined for microscopic wall-wall separation. With the present definition of the effective width h, water may have a monolayer structure if $h \sim 0$, a bilayer structure if $h \sim \sigma$, and so on, where σ is the molecular "diameter" of water.

MD simulations in the isothermal and isostress ensemble or $NP_{xx}(=P_{yy})T$ ensemble are performed, where P_{xx} and P_{yy} are the components of pressure tensor normal to the yz and xz planes, respectively, to which we shall refer as the lateral pressure, and T is the temperature. This ensemble is not isos-
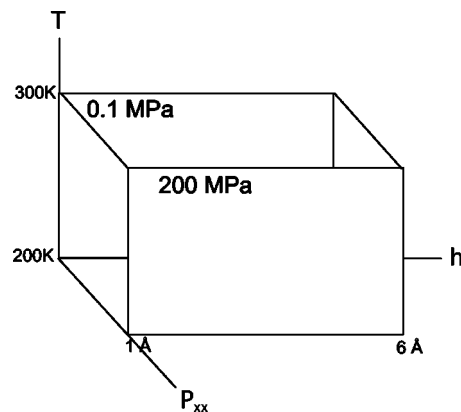
FIG. 2. Isostress h-T planes in which phase behavior of confined water is examined.

tress to the component P_{zz} of pressure tensor normal to the walls, for the effective width h is kept fixed. The isothermal-isostress MD simulation is more efficient than other MD simulations in examining phase behavior and phase transitions of a liquid confined in a rigid slit pore. Implementation of the $NP_{xx}(=P_{yy})T$ ensemble simulation is a straightforward extension of the standard isothermal-isobaric MD simulation;[23] here the lateral dimensions L_x and L_y vary in response to the corresponding lateral pressures being kept fixed at a given value while the width h is kept fixed.

A thermodynamic state of the one-component system is specified by three variables, which are taken to be T, h, and P_{xx}. Our main goal is to reveal the phase behavior of confined water in a part of the three-dimensional thermodynamic space, in which both the bilayer and monolayer solid phases are involved. To this end we choose two isostress planes, $P_{xx} = 200$ MPa and $P_{xx} = 0.1$ MPa, and apply the MD simulation at thermodynamic states corresponding to grid points of a square net within a rectangular region of $200K \leqslant T \leqslant 270$ K and 1.3 Å $\leqslant h \leqslant 6.0$ Å for each isostress plane. Figure 2 shows the two rectangular regions. Neighboring grid points are 0.1 Å or 0.2 Å apart for h and 5 or 10 K apart for T. In addition, thermodynamic states at $h = 7, 8, \ldots, 20$ Å and at $P_{xx} = 0.1$ MPa and $T = 200$ K are examined.

The number N of molecules is taken to be 240 for the states with $h \leqslant 10$ Å and 480 otherwise; then the lateral dimensions L_x and L_y of the simulation box are larger than 30 Å at any examined conditions. The Gear predictor-corrector method is employed for solving the equation of motion with a time step of 0.5 fs.

The following procedure is taken to determine the melting and freezing curves on each of the two isostress planes. First we perform preliminary MD simulations to find out some values of h at which the liquid water spontaneously freezes into the monolayer ice or into the bilayer amorphous ice when T decreases from 270 K to 200 K. Then we choose one of such states as a starting point (e.g., $h = 1.5$ Å and $T = 200$ K for the monolayer ice phase). Second we perform MD simulations of 10 ns each at the neighboring grid points using a final configuration of molecules at the starting point and then check the structure, the potential energy, and other properties. In most cases it is easy to judge whether the system undergoes a phase change or remains in the same state at

a given condition; otherwise we extend the simulation up to 100 ns at the same condition. The second step is repeated by encompassing the grid points until the solid phase melts or transforms into the other solid phase. This set of MD simulations determines the melting curve (or the stability limit) of the solid phase. Once the melting curves are obtained it is easy to find the freezing curves. The system in a liquid state at the melting point at given h is cooled by 5 K and is examined if it freezes at that temperature within 20 ns. If there is any sign of freezing the MD simulation is extended until the system freezes completely; if there is no sign of freezing, the temperature is further decreased in steps until spontaneous freezing is observed. This set of MD simulations are done at each value of h in the grid points. At some values of h the liquid water never freezes at and above 200 K. Then the value of h is increased or decreased in steps at that temperature until the system freezes spontaneously. From these MD simulations the freezing curves are determined at each isostress plane.

It is worthwhile here to make some remarks on the employment of the TIP4P model for water-water interaction and the LJ 9-3 model for the water-wall interactions. The bilayer ice and the bilayer amorphous have been obtained from the simulations of the ST2 and TIP5P models.[24] As mentioned earlier the monolayer ice has been obtained from the TIP5P water.[16] The LJ 9-3 potential for the water-wall interaction ignores any atomic structure of the walls, but it was confirmed from our earlier simulations that a potential function representing structure of hydrophobic surfaces gives rise to the same structure of the bilayer ice. (Note in the case the normal pressure is fixed.) Therefore, the results presented below would not be qualitatively altered by use of other reasonable potential models for water and hydrophobic surfaces.

III. THERMODYNAMICS FOR THE CONFINED SYSTEM

Thermodynamic identities for the one-component system having the quasi-two-dimensional geometry under the $NP_{xx}T$ ensemble are summarized here. For the thermodynamics of confined fluids in an open environment the reader should refer to the paper by Evans and Marini Bettolo Marconi.[1]

The infinitesimal change in the internal energy U of the confined system [Fig. 1] is written as

$$dU = TdS - AP_{zz}dh - P_{xx}hdA + \mu dN, \qquad (3)$$

and when N, P_{xx}, h, and T are fixed the natural choice of the thermodynamic potential is

$$\Phi = U + AhP_{xx} - TS. \qquad (4)$$

Then its differential is given by

$$d\Phi = -SdT - A\Delta Pdh + AhdP_{xx} + \mu dN, \qquad (5)$$

where $\Delta P = P_{zz} - P_{xx}$. From the general condition

$$\delta T\delta S - \delta(AP_{zz})\delta h - \delta(hP_{xx})\delta A + \delta N\delta\mu \geq 0 \qquad (6)$$

for the stability of this system, we find

$$(\partial AP_{zz}/\partial h)_{P_{xx}} + P_{xx}(\partial A/\partial h)_{P_{xx}} \leq 0, \quad (\partial A/\partial P_{xx})_h \leq 0 \quad (7)$$

with fixed T and N, in addition to $(\partial S/\partial T)_{h,P_{xx},N} \geq 0$ and $(\partial\mu/\partial N)_{T,P_{xx},h} \geq 0$. These conditions determine the signs of the second derivatives of Φ:

$$\partial^2\Phi/\partial T^2 \leq 0, \quad \partial^2\Phi/\partial P_{xx}^2 \leq 0, \quad \partial^2\Phi/\partial N^2 \geq 0;$$

however they do not determine the sign of $\partial^2\Phi/\partial h^2$ or $(\partial A\Delta P/\partial h)_{P_{xx}}$. Indeed, from the first inequality in Eq. (7),

$$(\partial A\Delta P/\partial h)_{P_{xx}} \leq -2P_{xx}(\partial A/\partial h)_{P_{xx}},$$

the right-hand side of which can be either positive or negative.

Since Φ is a homogeneous first-order function of N with fixed T, h, and P_{xx}, integrating Eq. (5) gives

$$\Phi = \mu N. \qquad (8)$$

This combined with Eq. (5) results in the Gibbs–Duhem equation for the confined system:

$$d\mu = -sdT - a\Delta Pdh + vdP_{xx}, \qquad (9)$$

where $s = S/N$, $a = A/N$, and $v = Ah/N = V/N$. Then we find from Eq. (9) the following Maxwell relations: for a fixed lateral pressure P_{xx},

$$\left(\frac{\partial s}{\partial h}\right)_{P_{xx},T} = \left(\frac{\partial a\Delta P}{\partial T}\right)_{P_{xx},h}, \qquad (10)$$

for a fixed width h,

$$\left(\frac{\partial s}{\partial P_{xx}}\right)_{h,T} = -\left(\frac{\partial v}{\partial T}\right)_{h,P_{xx}}, \qquad (11)$$

and for a fixed temperature T,

$$\left(\frac{\partial v}{\partial h}\right)_{T,P_{xx}} = -\left(\frac{\partial a\Delta P}{\partial P_{xx}}\right)_{T,h}. \qquad (12)$$

Equilibrium conditions for any two distinct phases α and β under the $NP_{xx}T$ ensemble are $T^\alpha = T^\beta$, $\mu^\alpha = \mu^\beta$, and $P_{xx}^\alpha = P_{xx}^\beta$. Note that in general $P_{zz}^\alpha \neq P_{zz}^\beta$ at equilibrium.

A two-phase boundary of the present system is a surface in the three-dimensional thermodynamic space, and the slopes of the surface at fixed h, T, and P_{xx} are given, respectively, by

$$\left(\frac{\partial T}{\partial P_{xx}}\right)_h = \frac{v^\alpha - v^\beta}{s^\alpha - s^\beta}, \qquad (13)$$

$$\left(\frac{\partial P_{xx}}{\partial h}\right)_T = \frac{(a\Delta P)^\alpha - (a\Delta P)^\beta}{v^\alpha - v^\beta}, \qquad (14)$$

and

$$\left(\frac{\partial h}{\partial T}\right)_{P_{xx}} = -\frac{s^\alpha - s^\beta}{(a\Delta P)^\alpha - (a\Delta P)^\beta}, \qquad (15)$$

which are the Clapeyron equations for the two-phase boundaries in the quasi-two-dimensional system. The triple point at which three phases α, β, and γ are in equilibrium is a triple "line" in the three-dimensional (3D) thermodynamic space. Since $d\mu^\alpha = d\mu^\beta$ and $d\mu^\beta = d\mu^\gamma$ along the triple line and each

$d\mu$ is given by Eq. (9), the direction of the triple line is uniquely determined. Let $\Delta_1 x$ and $\Delta_2 x$ denote the differences $x^\alpha - x^\beta$ and $x^\beta - x^\gamma$, respectively, for any quantity x of each phase. Then the direction of the triple line is expressed as

$$\frac{dT}{dP_{xx}} = \frac{\Delta_1 v \Delta_2(a\Delta P) - \Delta_2 v \Delta_1(a\Delta P)}{\Delta_1 s \Delta_2(a\Delta P) - \Delta_2 s \Delta_1(a\Delta P)} \quad (16)$$

and

$$\frac{dh}{dP_{xx}} = \frac{\Delta_1 v \Delta_2 s - \Delta_2 v \Delta_1 s}{\Delta_1 s \Delta_2(a\Delta P) - \Delta_2 s \Delta_1(a\Delta P)}. \quad (17)$$

This is a set of Clapeyron equations for the triple line.

The Clapeyron equations can be used to check the results of MD simulations and, when combined with them, provide an effective route to determination of the two-phase boundaries and the triple line in the 3D thermodynamic space.

IV. FORMATION AND STRUCTURE OF MONOLAYER ICE

Apart from a single MD simulation at each of the grid points to determine phase boundaries, ten independent MD simulations at a representative thermodynamic point ($h = 2.3$ Å, $T = 250$ K, and $P_{xx} = 200$ MPa) are performed to examine formation and structure of the monolayer ice. Initial configurations of water molecules are those of liquid water at 270 K with the same h and P_{xx} and a trajectory of 30 ns is generated in each simulation and if freezing is observed it is extended by 20 ns. It is found that the probability of freezing into the monolayer ice within 30 ns is 80%. The phase change accompanies significant decrease in the potential energy. The average potential energy of the "metastable" liquid state is -36.9 kJ/mol whereas that of the low-energy phase is -41.6 kJ/mol. (The latter value is the average over the last 20 ns of a single trajectory of 50 ns.) The decrease in potential energy, 4.7 kJ/mol, is as large as 80% of the latent heat of ice Ih.

The "lateral" radial distribution functions $g_{oo}(r)$s for oxygen atoms of the inherent structures are plotted in Fig. 3, where $r = \sqrt{(\Delta x)^2 + (\Delta y)^2}$ with Δx and Δy being the difference in the x and y coordinates of two oxygen atoms. The inherent structure is a potential-energy local minimum structure obtained by applying the steepest descent method to an instantaneous structure generated from an MD simulation. It is often more convenient to use the inherent structure for structural analyses than the instantaneous structure because fluctuations due to thermal motions are absent in the former. It is clear that the liquid phase does not have a long-range order even in the inherent structure whereas the monolayer ice phase does have sharp peaks and valleys in the entire range of r. In the monolayer ice phase the first and second peaks of $g_{oo}(r)$ correspond to hydrogen-bonding pairs of oxygen atoms whereas in the liquid phase only the first peak corresponds to hydrogen-bonding pairs. The first and second peaks for the monolayer ice are located at 2.3 and 2.8 Å, respectively, and some of other peaks are found at distances of multiples of 2.3 Å and those of 2.8 Å. The transverse distance of 2.8 Å is close to and that of 2.3 Å is much
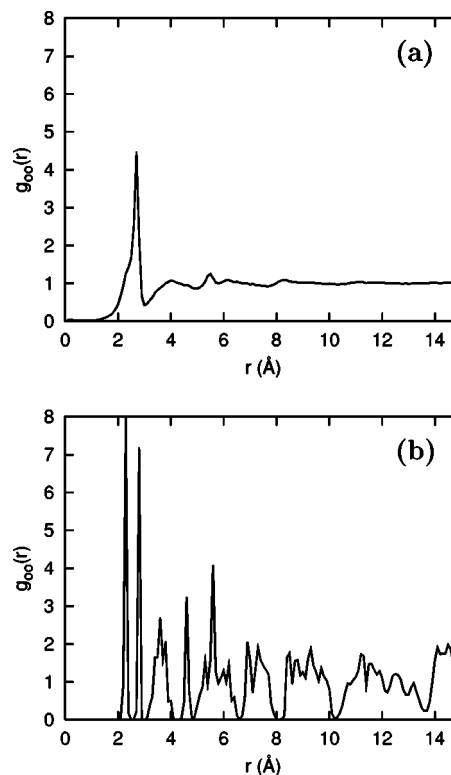
FIG. 3. The lateral radial distribution functions for oxygen atoms of the inherent structure: (a) liquid and (b) monolayer ice, both of which are obtained from the instantaneous structures at $T = 250$ K, $P_{xx} = 50$ MPa, and $h = 2.3$ Å.

shorter than the typical distance of a hydrogen-bonding pair of oxygen atoms. This indicates that one type of the hydrogen bonds is nearly parallel to the walls and the other forms an angle with the walls.

We define here the hydrogen bond in the inherent structure such that a pair of molecules is hydrogen bonded with each other if the pair potential energy ϕ is less than -12 kJ/mol. Then it is found that each molecule in the monolayer ice phase is bonded with its four nearest neighbors, with some exceptions, as in ice Ih. What seems to be unique for the monolayer ice is that the distribution of the hydrogen-bond energy has four distinct peaks as shown in Fig. 4. They are located at -24.6, -22.6, -18.0, and -14.6 kJ/mol.
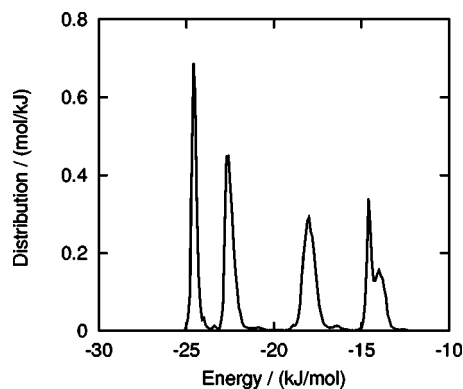
FIG. 4. Distribution of the hydrogen-bond energy in the monolayer ice (obtained from the same inherent structures as in Fig. 3.
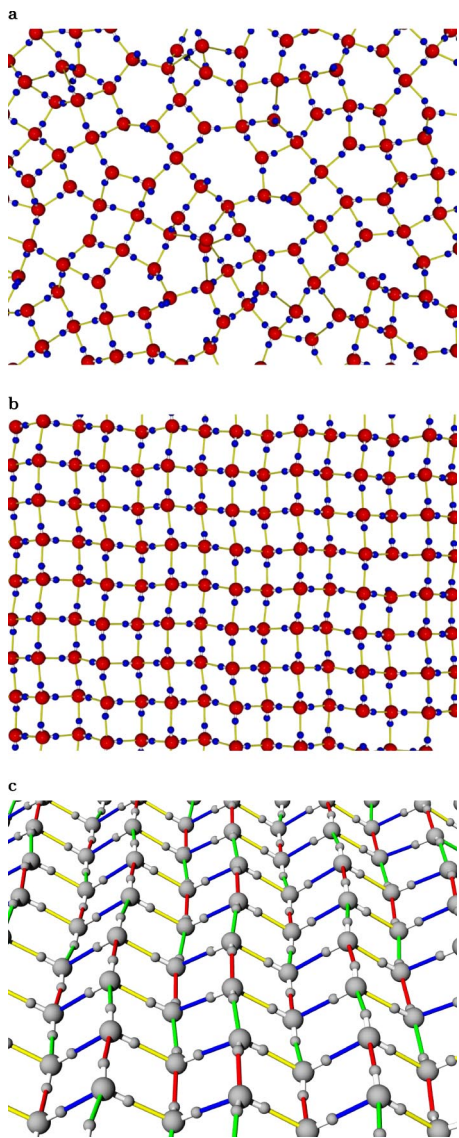
FIG. 5. Inherent structures of (a) the high-energy phase, (b) the low-energy phase, and (c) the low-energy phase viewed from an acute angle to the walls.

Figure 5 shows an inherent structure of the high-energy phase and that of the low-energy phase. It is clear from the pictures taken from a direction normal to the walls [Figs. 5(a) and 5(b)] that the high-energy phase is a liquid with a disordered hydrogen-bond network whereas the low-energy phase is a monolayer crystalline solid with a nearly perfect network. The in-plane structure of the monolayer ice looks like a rectangular net: each node of the net has an oxygen atom and each bond has a hydrogen atom, and the ice rule is satisfied over the entire net except some points of defects. This is essentially realization of the two-dimensional ice model,[25] which has been studied as one of exactly solvable models in statistical mechanics, not as a realistic model of two-dimensional ice. The structure of monolayer ice is, however, not exactly two-dimensional: a view [Fig. 5(c)] from an acute angle to the walls shows a puckered structure of the monolayer. The straight rows forming ridges and valleys of the puckered structure have the horizontal hydrogen bonds. The zigzag rows crossing over the folds have the hydrogen

bonds tilting with respect to the walls. The distribution of the hydrogen-bond length has two peaks centered at 2.74 Å and 2.83 Å and the former corresponds to the horizontal bonds and the latter to the tilting bonds.

Any ice form in which the molecular structure of water remains intact satisfies the ice rule to have a perfect hydrogen-bond network; the monolayer ice is not an exception. If there are no other restrictions on the proton arrangement, the residual entropy of the monolayer ice would be exactly the same as that of the two-dimensional ice model: $k \ln(4/3)^{3/2}$, which is the exact value obtained by Lieb.[25] However, there is obviously some restrictions other than the ice rule. First, two protons of each molecule cannot participate in the two hydrogen bonds along the straight row at the same time because the hydrogen-bond angle 180° is far greater than the HOH angle. Second, they also cannot participate in the two bonds along the zigzag row at the same time because a perfect hydrogen-bond network containing such molecules must also contain molecules violating the first rule. Consequently each molecule has four possible orientations in each of which one of its proton participates in one of the two hydrogen bonds along the straight row and the other participates in one of the two bonds along the zigzag row. Then there are only two possible arrangements for a set of all protons on each row. The number of such rows are $2\sqrt{N}$ provided the number of straight rows and that of the zigzag rows are the same. Therefore the residual entropy is

$$S = k \ln 2^{2\sqrt{N}}, \tag{18}$$

which is subextensive and therefore S/N goes to zero in the thermodynamic limit. It should be noted that Pauling's approach to the residual entropy of ice is an approximation (an excellent approximation for ice Ih) but it may lead to a wrong result for some ices. For example, the two-dimensional ice model, which has no restrictions on its proton arrangement other than the ice rule, would have exactly the same residual entropy as that of ice Ih if it is evaluated by Pauling's method; but we know the former is $k \ln(4/3)^{3/2}$ and the latter is nearly equal to $k \ln(3/2)$. For the monolayer ice, which has additional restrictions on the proton arrangement, Pauling's method gives rise to a "negative" residual entropy: $k \ln W$ with $W < 1$, which is irrational.[16] But because of the additional restrictions one can count W exactly with no effort as given in Eq. (18).

The monolayer ice obtained from any reasonable intermolecular potential model of water, or the real one yet to be discovered, would satisfy the ice rule and the additional restrictions. But whether any further restriction applies or not may be model dependent and should wait for experimental observation. In the case of the TIP4P model (with the switching function) the monolayer ice resulting from spontaneous freezing tends to have a structure in which the two possible arrangements, say A and B, for a set of protons in each row appear regularly as AABB···, as shown in Figs. 5(b) and 5(c). The simulation of the TIP5P water predicted the AAAA structure.[16]

Figure 5(c) shows the strength of each hydrogen bond dividing into four energy levels: strongest ($\phi < -30.0$), stronger ($-30.0 < \phi < -23.6$), weaker ($-23.6 < \phi < -16.0$), and
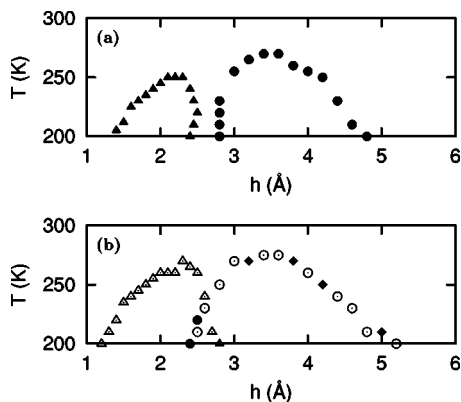
FIG. 6. Diagrams of spontaneous freezing (a) and melting (b) observed in the h-T plane at $P_{xx}=200$ MPa.

FIG. 7. Diagrams of spontaneous freezing (a) and melting (b) observed in the h-T plane at $P_{xx}=0.1$ MPa.

weakest $(-16.0<\phi)$, all in units of kJ/mol. Half the tilting bonds along the zigzag rows are the strongest hydrogen bonds (blue bonds in the figure) and the other half are the weaker bonds (yellow); half the horizontal bonds along the straight rows are the stronger bonds (green) and the other half are weakest bonds (red). It is clear from the figure that the four energy levels of hydrogen bonds (shown in Fig. 4) correspond to four relative orientations of bonding pairs. The strongest bonds connect two neighboring straight rows one of which is in state A and the other is in state B (the same A and B defined above), so the dipole-dipole interaction of each pair is energetically favorable. On the other hand, the weaker bonds connect two neighboring straight rows both in state A or B, so the dipole-dipole interaction is unfavorable. Similarly, the weakest bonds connect two neighboring zigzag rows both in state A or B and thus each bonding pair has the same orientation (so the higher interaction energy) while the stronger bonds connect two zigzag rows in states A and B and so the dipole-dipole interaction is more favorable. This completes structural analyses of the monolayer ice.

V. FREEZING, MELTING, AND STRUCTURAL CHANGE

A large number of MD simulations performed at grid points on an isostress plane, each starting from a liquid state, reveal a series of points at which liquid water freezes spontaneously. That is, a freezing curve in the h-T plane is approximately identified by this procedure. Likewise, MD simulations at grid points starting from a solid state identify a melting curve of that solid in the h-T plane.

Figure 6(a) shows freezing points in the isostress plane of 200 MPa. It is clearly shown that there are two separate domains in which spontaneous freezing takes place; the resulting phase is the monolayer ice in the domain located at smaller-h side and the bilayer amorphous solid in the other domain at larger-h side. The domain of the bilayer phase is significantly larger than that of the monolayer ice. The highest freezing point is 270 K at h between 3.4 and 3.6 Å for the bilayer solid whereas it is 250 K at h between 2.1 and 2.3 Å for the monolayer ice. At 200 K, the range of h of the bilayer domain is twice as wide ([2.8 Å, 4.8 Å]) as that of the monolayer domain ([1.4 Å, 2.4 Å]). There is a gap between the two domains, ranging from 2.5 to 2.8 Å at 200 K,
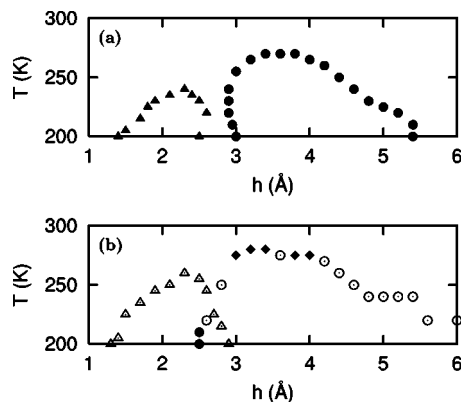
where the confined water remains to be a liquid even at 200 K. (Strictly speaking, freezing is not observed in the MD simulation of 100 ns.)

In Fig. 6(b) displayed are a series of melting points for the monolayer ice and that for the bilayer amorphous phase in the same isostress plane as in Fig. 6(a). The domain under the melting "curve" is again larger for the bilayer phase than for the monolayer ice phase; the highest melting point is 280 K at h between 3.2 and 3.8 Å for the bilayer amorphous and 270 K at h between 2.3 and 2.4 Å for the monolayer ice. In some cases the bilayer amorphous phase does not melt but transforms itself into the bilayer crystal in the course of raising temperature at fixed h (e.g., 270 K at 3.2 or 3.8 Å). It is also found that the two melting curves cross at around $(h,T)=2.6$ Å, 230 K and thus there is an overlap of the monolayer ice and bilayer amorphous domains. Indeed, the system undergoes the structural change from the bilayer amorphous to the monolayer ice at 2.4 Å, 200 K and at 2.5 Å, 220 K and the reverse structural change at 2.8 Å, 200 K.

Figure 7 shows freezing points and melting points in the isostress plane of 0.1 MPa. The freezing and melting curves are similar to those at 200 MPa. However, several systematic deviations are caused by the change of the lateral pressure P_{xx}. First, both the freezing and melting points of the monolayer ice decreases with decreasing pressure when h is less than 2.4 Å. The highest freezing point is 240 K and the highest melting point is 260 K (both at 2.3 Å), which are both lower than those at 200 MPa. Second, although the highest freezing point and the highest melting point of the bilayer amorphous phase are nearly independent of the pressure, both freezing and melting points at $h>3.8$ Å increase with decreasing P_{xx}; the largest possible h for the spontaneous freezing at 200 K increases from 4.8 to 5.4 Å with decreasing P_{xx} from 200 to 0.1 MPa. We again observe that in some cases the bilayer amorphous phase does not melt but transforms itself into the bilayer ice phase in the heating process. As observed at 200 MPa, the melting curves of the monolayer ice and the bilayer amorphous phases cross and the structural transformation between two solid phases takes place.

Summing up the effects of pressure shown in Figs. 6 and

TABLE I. Phase equilibria among α (liquid water), β (bilayer ice), and γ (monolayer ice). Thermodynamic quantities are evaluated at representative points A, B, C, D, E at P_{xx}=200 MPa and F, G, H, I, J at P_{xx} =0.1 MPa. Difference Δx at the κ-λ equilibrium is defined as $x^{\kappa}-x^{\lambda}$, where $x=u,s,\ldots$ and $\kappa,\lambda=\alpha,\beta,\gamma$. h is in units of Å, T in units of K, u in units of kJ mol^{-1}, s in units of J mol^{-1} K^{-1}, v in units of Å^3, and $a\Delta P$ in units of Å^2 MPa.

Point	(h, T)	Equilibrium	Δu	Δs	Δv	$\Delta(a\Delta P)$	$\partial T/\partial P_{xx}$	$\partial P_{xx}/\partial h$	$\partial T/\partial h$
A	(1.4, 210)	α-γ	3.45	17.2	1.33	-3.28×10^3	0.0466	-2.47×10^3	115
B	(2.3, 260)	α-γ	5.29	21.2	1.76	531	0.0502	3.02×10^2	-15.1
C	(2.5, 230)	α-γ	1.16	4.30	-1.39	5.48×10^3	-0.195	-3.94×10^3	-767
D	(2.8, 240)	α-β	3.46	14.7	0.496	-3.24×10^3	0.0204	-6.54×10^3	133
E	(3.6, 270)	α-β	3.93	14.2	-0.753	413	-0.0319	-5.49×10^2	-17.5
F	(4.6, 220)	α-β	2.24	8.84	-2.47	1.20×10^3	-0.169	-4.84×10^2	-81.5
G	(1.4, 200)	α-γ	3.60	18.0	1.38	-2.74×10^3	0.0462	-1.98×10^3	91.6
H	(2.3, 245)	α-γ	5.43	22.2	2.36	99.2	0.0640	4.21×10^2	-2.69
I	(2.5, 240)	α-γ	4.05	16.9	1.01	1.84×10^3	0.0360	1.83×10^3	-65.9
J	(2.8, 220)	α-β	2.00	9.11	0.976	-3.94×10^3	0.0645	-4.04×10^3	261
K	(3.6, 270)	α-β	4.12	15.2	-0.157	194	-0.0062	-1.24×10^3	-7.66
L	(4.6, 245)	α-β	3.84	15.7	-1.46	906	-0.0559	-6.22×10^2	-34.8

7, the domain of the monolayer ice in the h-T plane shrinks. In contrast, the domain of the bilayer amorphous solid expands with decreasing pressure.

VI. PHASE EQUILIBRIA OF CONFINED WATER

Let now α, β, and γ stand for the liquid phase, the bilayer amorphous phase, and the monolayer ice phase, respectively. The direct observation of melting and freezing transitions of the confined water allows us to narrow down the α-β and α-γ two-phase equilibrium T at given h and P_{xx} or equilibrium h at given T and P_{xx}. Uncertainty in the equilibrium T (or h) is the difference in T (or h) between the point of spontaneous freezing and that of spontaneous melting. It is found that the smallest uncertainty in T is only 5 K, the same as the smallest increment (or decrement) in T chosen in the MD simulations, and the smallest uncertainty in h is 0.1 Å. The uncertainty is relatively large when two phases are expected to coexist at low T, for the lower the temperature the lower the nucleation rate of a new phase.

In some cases, we can still reduce the uncertainty from thermodynamic requirement. For example, let us look at the point: h=2.55 Å, T=200 K, and P_{xx}=200 MPa, where neither spontaneous freezing of the liquid nor spontaneous melting of the monolayer ice is observed. From Eqs. (4) and (8) $\mu^{\alpha}-\mu^{\beta}=\psi^{\alpha}-\psi^{\beta}-T(s^{\alpha}-s^{\beta})$ with $\psi=(U+AhP_{xx})/N$, the quantity corresponding to the enthalpy per molecule for the bulk system. Both ψ^{α} and ψ^{β} are directly obtained from MD simulations, and we find $\psi^{\alpha}-\psi^{\beta}<0$ at this particular point. But at the same time we know $s^{\alpha}-s^{\beta}>0$. Therefore $\mu^{\alpha}<\mu^{\beta}$, i.e., the liquid must be the stable state at this point. Since the liquid freezes at T=220 K and h=2.5 Å, we may conclude that the true equilibrium h at 200 K and 200 MPa is between 2.50 and 2.55 Å, the uncertainty being only 0.05 Å.

In order to determine the two-phase boundaries in each isostress plane and ultimately the two-phase surfaces in the 3D thermodynamic space, 12 points are chosen as representa-tive α-β and α-γ equilibrium states. Each point is either a melting point, a freezing point, or a midpoint between melting and freezing points.

Then the differences in u, s, v, and $a\Delta P$ between two phases are evaluated at these points. The entropy difference Δs is given as $\Delta\psi/T=\Delta u+P_{xx}\Delta v$ with the assumption that $\Delta\mu=0$ at these points. The results are shown in Table I. By Eqs. (13)–(15), the slopes of the phase boundaries are related with the ratio of differences in s, v, and $a\Delta P$ between two coexisting phases. Evaluated values of the slopes $(\partial T/\partial P_{xx})_h$, $(\partial P_{xx}/\partial h)_T$, and $(\partial h/\partial T)_{P_{xx}}$ at the 12 points are also listed in Table I. Phase boundaries in the h-T planes are determined by interpolating the 12 points with the information of $(\partial h/\partial T)_{P_{xx}}$ at these points.

VII. PHASE DIAGRAMS IN THE h-T PLANE

Figure 8 shows the phase diagrams at 200 MPa and 0.1 MPa. The phase diagrams and Table I give significant amount of information. The first and obvious is that the domain of the bilayer amorphous solid phase β at a given pressure is larger than that of the monolayer solid phase γ at that pressure, as we have seen in Figs. 6 and 7. The domain of the γ phase becomes smaller while that of the β phase becomes larger with decreasing P_{xx} from 200 MPa to 0.1 MPa, and so the size difference between the two domains is pronounced at the ambient pressure.

The second is that the width of each loop, i.e., the range of h in which each solid is the stable phase, monotonically shrinks with increasing T and eventually disappears at the highest melting temperature of that solid phase. More precisely, the slope of each loop is always positive on the smaller-h side and always negative on the larger-h side. Since the slope is given by Eq. (15) and the entropy difference $s^{\text{liq}}-s^{\text{sol}}$ between liquid and solid phases in equilibrium is always positive, the slope is positive (negative) if $(a\Delta P)^{\text{liq}}-(a\Delta P)^{\text{sol}}$ is negative (positive). Table I shows $(a\Delta P)^{\text{liq}}-(a\Delta P)^{\text{sol}}$ is positive on the larger-h sides (points C, F, I, and L) and negative on the smaller-h sides (points A, D,
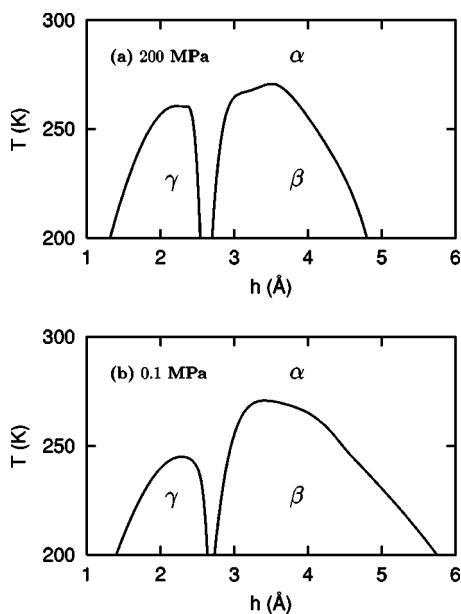
FIG. 8. Phase diagram of confined water: (a) $P_{xx}=200$ MPa and (b) $P_{xx}=0.1$ MPa. The symbols α, β, and γ indicate the liquid, bilayer solid, and monolayer solid phases, respectively.

FIG. 9. Normal pressure P_{zz} on the walls as a function of h: (a) 260 K and (b) 240 K. The lateral pressure P_{zz} is fixed at 0.1 MPa.

G, and J). The same results would be expected for any quasi-two-dimensional system that exhibits liquid-solid phase transitions under low or moderate lateral pressure. To see this, let f_z be a normal force per molecule acting on the wall. If P_{xx} is small compared to P_{zz} in the liquid or solid phase, which is always the case in our simulations, $(a\Delta P)^{\text{liq}}-(a\Delta P)^{\text{sol}}\simeq f_z^{\text{liq}}-f_z^{\text{sol}}$. The phase change caused by decreasing h (so increasing f_z) should be in the direction that reduces the stress, i.e., decreases f_z. Thus, $f_z^{\text{liq}}-f_z^{\text{sol}}>0$ on the larger-h side of the liquid-solid boundary whereas $f_z^{\text{liq}}-f_z^{\text{sol}}<0$ on the smaller-h side. It is, therefore, generally expected for the system under low or moderate lateral pressure that the slope $\partial T/\partial h$ of a solid-liquid phase boundary is always positive on the small-h side and is always negative on the other side. It is now clear that each loop is smooth everywhere including the point where the small-h and large-h phase boundaries meet at the highest melting temperature. [The shape of the β loop has been inferred from our earlier MD simulations (see Fig. 6b in Ref. 15).] At the highest melting point, where $\partial T/\partial h=0$, $(a\Delta P)^{\text{liq}}=(a\Delta P)^{\text{sol}}$ [Eq. (15)] and in particular $f_z^{\text{liq}}=f_z^{\text{sol}}$ if $P_{zz}\gg P_{xx}$.

The third is that the slope is much steeper on the inner side of each loop where the β and γ domains face each other than on the outer side of each loop (the left side of the γ domain and the right side of the β domain), which is again clearly shown in Fig. 8. The reason is less obvious and differs in the two cases. Steepness of the slope is determined by the magnitudes of Δs and $\Delta(a\Delta P)$. As to the β loop, $|\Delta(a\Delta P)|$ is much larger on the inner side than on the outer side while Δs differs very little on both sides (compare points D and F or J and L in Table I), which is the reason of the steeper slope on the inner side. As to the γ loop, on the other hand, the reason is that Δs is much smaller on the inner side than on the outer side while $|\Delta(a\Delta P)|$ is more or less the same on both sides (compare A and B in the table). Because
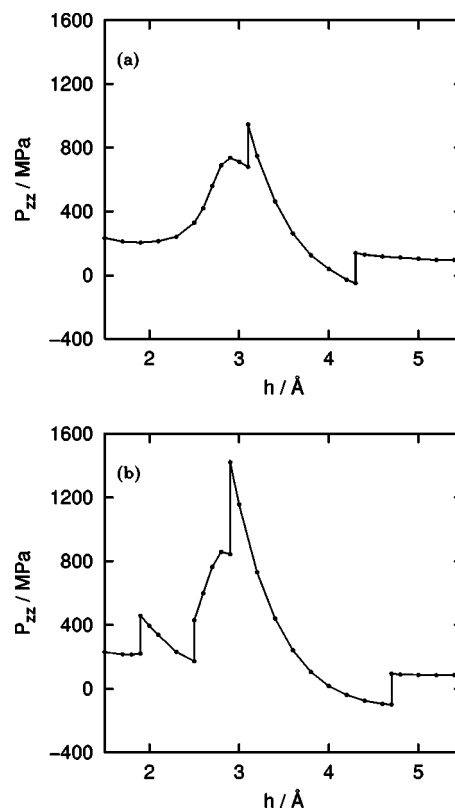
of their steep slopes, the α-β and α-γ phase boundaries on the inner sides do not meet in the temperature range above 200 K, i.e., the temperature of the α-β-γ triple point (at 0.1 MPa and 200 MPa) is lower than 200 K. The reason that the system undergoes the β-γ structural change above 200 K at 0.1 and 200 MPa is that at such temperatures the metastable region of the bilayer (monolayer) solid phase extends beyond the region of the liquid phase to the region of the monolayer (bilayer) solid phase.

Figure 9 shows the normal pressure P_{zz} acting on the walls as a function of h at fixed T (either 260 or 240 K) and fixed P_{xx} (0.1 MPa). At 260 K, the force curve exhibits a pair of discontinuities, between which the system is in the bilayer ice phase β and otherwise in the liquid phase α. The normal pressure P_{zz} increases monotonically and rapidly with decreasing h when the system is in the solid phase whereas the curve of P_{zz} shows a local maximum and minimum reflecting layering structure of the liquid. Note that the magnitude of P_{zz} is much greater than that of fixed P_{xx}, as mentioned above. Along the isothermal pass of 240 K, the force curve exhibits another pair of discontinuities between which the system is in the monolayer ice phase, and now the range where the system is in the bilayer ice phase is wider than at 260 K. These results are consistent with the phase diagram shown in Fig. 8(b).

VIII. GLOBAL PHASE DIAGRAM

Table I and Fig. 8 suggest that pressure dependence of the solid-liquid phase equilibria is simple and small. Thus a global phase diagram, i.e., a three-dimensional diagram in

the P_{xx}-h-T space, is obtained with reasonable accuracy by simply interpolating phase diagrams at the two isostress planes (P_{xx}=0.1 and 200 MPa), using derivatives of the equilibrium T or h with respect to P_{xx}. The resulting surfaces of the phase boundaries are displayed in Fig. 10.

It is found that the α-β equilibrium T at h=4.6 Å decreases with increasing P_{xx} (like the melting curve of ice Ih), whereas the equilibrium T at h=2.8 Å increases with increasing P_{xx} (like the melting curve of most solids). This is because the confined water expands as it freezes into the bilayer solid on the large-h side of the β domain but it shrinks at the small-h side. The α-γ equilibrium T at h =2.5 Å initially increases with increasing P_{xx} before reaching its maximum and then decreases, which reflects the pressure dependence of the volume change on the large-h side of the γ domain. On the small-h side (h=1.4 Å), the α-γ equi-

librium T monotonically increases with increasing P_{xx} because water shrinks as it freezes on that side.

The α-β equilibrium h at 200 K decreases monotonically with increasing P_{xx} on both the branches of the phase boundary. This is because Δv and $\Delta(a\Delta P)$ have opposite signs in any case. The dependence on P_{xx} is noticeable on the large-h branch but it is practically undetectable on the small-h branch. The α-γ equilibrium h at 200 K is very weakly dependent on P_{xx} on both branches of the boundary.

IX. CONCLUDING REMARKS

A phase diagram of water confined in a hydrophobic slit pore is obtained based on extensive MD simulations combined with the Clapeyron equations for the quasi-two-dimensional system. There are two solid phases, the monolayer ice and the bilayer amorphous (or crystalline) ice, as well as a liquid phase in a small range of the effective width (0 Å$<$$h$$<$6 Å) above 200 K. The liquid-solid phase boundaries of the two solids are convex curves with respect to h in the isostress h-T planes (Fig. 8) and convex surfaces (again with respect to h) in the three-dimensional P_{xx}-h-T space (Fig. 10). It is explained based on a general argument why the solid-liquid phase boundary on the large-h side of each loop has always a negative slope and that on the small-h side has always a positive slope.

The monolayer ice has a smaller domain than the bilayer solid in a given isostress plane but the difference in domain size becomes smaller as the lateral pressure is increased from 0.1 to 200 MPa. The highest melting temperature is around 260 and 270 K for the monolayer and bilayer solid, respectively, and the range of h where each solid phase can be stable is of the order of subnanometer at lower temperatures. These conditions for the formation of monolayer and bilayer solids of water can well be achieved and controlled in the surface force apparatus, atomic force microscopy, or other modern experiments.

Structural analyses of the monolayer ice (obtained from the TIP4P model) show that there are four kinds of hydrogen bonds regularly arranged in the crystal [Fig. 5(c)]. The residual entropy of the monolayer ice differs from that of the 2D ice model and is exactly given by Eq. (18), which is subextensive. No freezing transition is observed, i.e., liquid water remains stable, in the range of 6 Å$<$$h$$<$20 Å at 200 K and 0.1 MPa within the time scale of simulations (e.g., 30 ns).
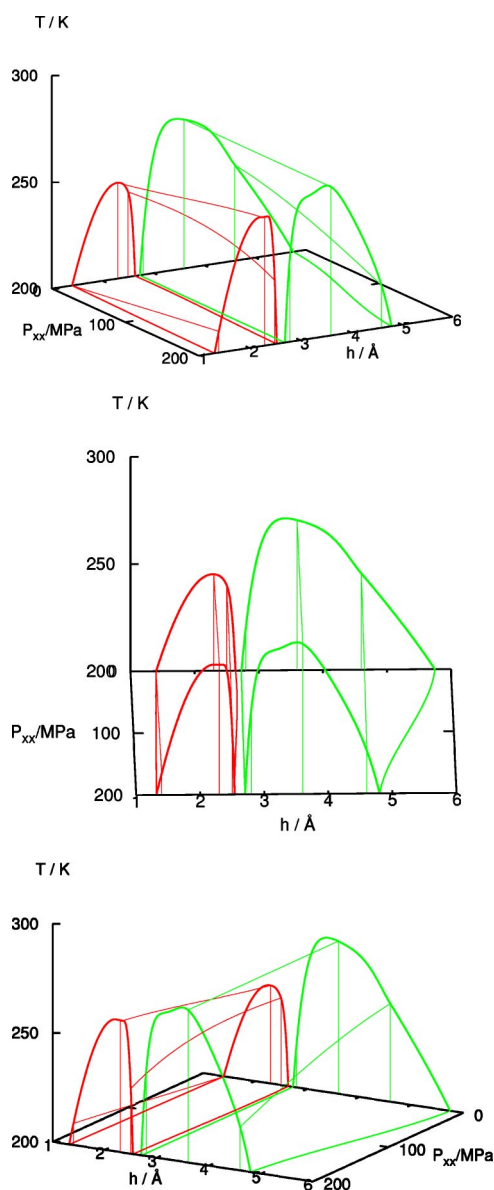
FIG. 10. Phase diagram of confined water in the three-dimensional P_{xx}-h-T space. Red and green curves are the phase boundaries of the monolayer ice and those of the bilayer (amorphous) ice, respectively. Thick curves are the equilibrium T as a function of h at given P_{xx} and thin curves are equilibrium T as a function of P_{xx} at given h.

[1] R. Evans and U. Marini Bettolo Marconi, J. Chem. Phys. **86**, 7138 (1987).
[2] R. Evans, J. Phys.: Condens. Matter **2**, 8989 (1990).
[3] L. D. Gelb, K. E. Gubbins, R. Radhakrishnan, and M. Sliwinska-Bartkowiak, Rep. Prog. Phys. **62**, 1573 (1999).
[4] C. Y. Lee, J. A. McCammon, and P. J. Rossky, J. Chem. Phys. **80**, 4448 (1984).
[5] S. H. Lee and P. J. Rossky, J. Chem. Phys. **100**, 3334 (1994).
[6] J. Hautman, J. W. Halley, and Y.-J. Rhee, J. Chem. Phys. **91**, 467 (1989).
[7] M. Watanabe, A. M. Brodsky, and W. P. Reinhardt, J. Phys. Chem. **95**,

4593 (1991).

[8] A. Delville, J. Phys. Chem. **97**, 9703 (1993).

[9] X. Xia and M. L. Berkowitz, Phys. Rev. Lett. **74**, 3193 (1995).

[10] J. C. Shelley and G. N. Patey, Mol. Phys. **88**, 385 (1996).

[11] K. Koga, X. C. Zeng, and H. Tanaka, Chem. Phys. Lett. **285**, 278 (1998).

[12] M. Meyer and H. E. Stanley, J. Phys. Chem. B **103**, 9728 (1999).

[13] K. Koga, X. C. Zeng, and H. Tanaka, Phys. Rev. Lett. **79**, 5262 (1997).

[14] K. Koga, H. Tanaka, and X. C. Zeng, Nature (London) **408**, 564 (2000).

[15] K. Koga, J. Chem. Phys. **116**, 10882 (2002).

[16] R. Zangi and A. E. Mark, Phys. Rev. Lett. **91**, 025502 (2003).

[17] K. Koga, G. T. Gao, H. Tanaka, and X. C. Zeng, Nature (London) **412**, 802 (2001).

[18] K. Koga, G. T. Gao, H. Tanaka, and X. C. Zeng, Physica A **314**, 462 (2002).

[19] Y. Maniwa, H. Kataura, M. Abe, S. Suzuki, Y. Achiba, H. Kira, and K. Matsuda, J. Phys. Soc. Jpn. **71**, 2863 (2002).

[20] W. L. Jorgensen, J. Chandrasekhar, J. D. Madura, R. W. Impey, and M. L. Klein, J. Chem. Phys. **79**, 926 (1983).

[21] I. Ohimine, H. Tanaka, and P. Wolynes, J. Chem. Phys. **89**, 5852 (1988).

[22] W. A. Steele, Surf. Sci. **36**, 317 (1973).

[23] S. Nosé, J. Chem. Phys. **81**, 511 (1984).

[24] J. Bai, X. C. Zeng, K. Koga, and H. Tanaka, Mol. Sim. **29**, 619 (2003).

[25] E. H. Lieb, Phys. Rev. Lett. **18**, 692 (1967).